JOURNAL OF BACTERIOLOGY, Aug. 2007, p. 6048–6056 Vol. 189, No. 16
0021-9193/07/$08.00+0 doi:10.1128/JB.00459-07

Integration of Rotation and Piston Motions in Coiled-Coil Signal Transduction▽

Rong Gao† and David G. Lynn*

Center for Fundamental and Applied Molecular Evolution, Departments of Chemistry and Biology, Emory University, Atlanta, Georgia 30322

Received 27 March 2007/Accepted 5 June 2007

A coordinated response to a complex and dynamic environment requires an organism to simultaneously monitor and interpret multiple signaling cues. In bacteria and some eukaryotes, environmental responses depend on the histidine autokinases (HKs). For example, VirA, a large integral membrane HK from *Agrobacterium tumefaciens*, regulates the expression of virulence genes in response to signals from multiple molecular classes (phenol, pH, and sugar). The ability of this pathogen to perceive inputs from different known host signals within a single protein receptor provides an opportunity to understand the mechanisms of signal integration. Here we exploited the conserved domain organization of the HKs and engineered chimeric kinases to explore the signaling mechanisms of phenol sensing and pH/sugar integration. Our data implicate a piston-assisted rotation of coiled coils for integration of multiple inputs and regulation of critical responses during pathogenesis.

Bacteria must interpret critical environmental shifts and fluctuations for successful adaptation and survival. The frontline responsibility for sensing many of these changes and mediating an appropriate response falls to the histidine autokinases (HKs). These sensor proteins control events ranging from osmotic regulation to pathogenesis via phosphotransfer from their conserved catalytic kinase core to a cognate response regulator (RR) (43, 55). The observation that several constructed chimeras of sensor kinase input and output domains remain functional (8, 49, 53) suggests that common signal perception and transmission mechanisms are operable across these signaling modules. However, the environmental signals that are recognized span many structural categories, and the responses to environmental fluctuations cover very different time scales. Moreover, precise adaptations to complex environments often necessitate the integration of information from multiple cues. Transcriptional coupling of two independent pathways (21), cross talk between HKs and RRs (2, 16), and phosphorelay across multiple components (37) may mediate more complex signaling tasks and signal integration mechanisms (9). Clearly, the identification of common regulator mechanisms within this complex regulatory architecture could clarify our understanding of the building blocks for prokaryotic signal processing and their modes of environmental adaptation.

The histidine kinase VirA, found in the plant pathogen *Agrobacterium tumefaciens*, activates the expression of virulence genes (*vir*) in response to host-derived signals from plant wound sites. Virulence constitutes the transfer of oncogenic DNA into host cells (30, 48, 57, 59) and requires phenols (e.g., acetosyringone [AS]), monosaccharides (including glucose), and an acidic pH (4.8 to 5.5) to fully initiate *vir* gene expression (57). VirA contains two signal input sites; the periplasmic domain is responsible for sensing low pH and monosaccharides, and the linker domain mediates phenol perception (12, 17). An additional C-terminal receiver domain also appears to be critical for response output to its cognate RR, VirG (13, 34). Perception of the information from these distinct input domains functions to activate the kinase domain for phosphotransfer to VirG.

Even with structurally defined signals and the domain structure of VirA delineated, the current lack of structural information and low homology of the linker to other structures have complicated mechanistic assignment of phenol activation. A proton transfer model has emerged largely from analyses of the diverse inducing phenols and designed inhibitors (24, 35). More recently, a coiled-coil-like region (Helix-C) positioned just after the second transmembrane segment (TM2) was identified as a region critical for phenol signaling (51). Fusion of the leucine zipper (LZ) of GCN4 at Helix-C was used to conformationally bias specific rotational interfaces. These chimeras display phenol-independent but rotational-interface-dependent activity, suggesting that the rotation of helices within a VirA dimer is important for phenol signaling. Similar helical rotation mechanisms have now been proposed for other HKs, including the yeast osmosensor Sln1 and the *Escherichia coli* ArcB sensor (22, 44), and recent structural information for HAMP domains further supports the importance of rotational ratcheting models (20).

In contrast, monosaccharide and pH perception is mediated by the periplasmic domain, and both signals are dependent on the sugar-binding protein ChvE (10, 38). These signals cannot activate the kinase in the absence of phenol, but in the presence of sugar and an acidic pH, *vir* expression levels and phenol sensitivity are greatly enhanced (39). Thus, the pH/sugar signal must be transduced through the membrane and integrated with the phenol-induced rotational mechanism.

Our studies attempting to understand the integration of

* Corresponding author. Mailing address: Center for Fundamental and Applied Molecular Evolution, Departments of Chemistry and Biology, Emory University, Atlanta, GA 30322. Phone: (404) 727-9348. Fax: (404) 727-6586. E-mail: dlynn2@emory.edu.

† Present address: Center for Advanced Biotechnology and Medicine, University of Medicine and Dentistry of New Jersey, Piscataway, NJ 08854.

▽ Published ahead of print on 15 June 2007.

TABLE 1. Bacterial strains and plasmids

Strain or plasmid	Relevant characteristics	Source or reference
E. coli strains		
XL1-Blue	*recA1 endA1 gyrA96 thi-1 hsdR17 supE44 relA1 lac*[F′ *proAB lacI*^{q}*ZΔM15* Tn*10* (Tc^r)]	Stratagene
DH5α	*recA1 endA1 hsdR17 supE44 gyrA96 relA1*Δ(*lacZYA-argF*)*U169* (ϕ80d*lacZΔM15*)	Invitrogen
A. tumefaciens strains		
A348-3	A136 containing pTiA6NC, Δ*virA*	23
A136	Strain C58 cured of pTi plasmid	54
Plasmids		
pYW15b	Broad-host-range expression vector, IncW, pBR322*ori*, Ap^r	52
pJZ4	P_{virB}-*lacZ* in pMON596, IncP Spec^r	17
pRG109	P_{N25}-His$_6$-*virG* in pJZ4, Spec^r	17
pSW209Ω	*virB*::*lacZ*, IncP Spec^r	52
pRG150	*lacI*^{q} in pJZ4, Spec^r	This study
pJM6	P_{N25}-His$_6$-*virG* in pRG150, Spec^r	27
pVRA8	*virA*, IncW, pBR322*ori*, Ap^r	23
pRG95	P_{N25}-His$_6$-LZ(4)-*virA*(*aa426-829*)(*G665D*) in pYW15b, Ap^r	This study
pRG96	P_{N25}-His$_6$-LZ(3)-*virA*(*aa426-829*)(*G665D*) in pYW15b, Ap^r	This study
pRG98	P_{N25}-His$_6$-LZ(0)-*virA*(*aa426-829*)(*G665D*) in pYW15b, Ap^r	This study
pRG178	P_{N25}-His$_6$-LZ(4)-*virA*(*aa426-711*)(*G665D*) in pYW15b, Ap^r	This study
pRG179	P_{N25}-His$_6$-LZ(3)-*virA*(*aa426-711*)(*G665D*) in pYW15b, Ap^r	This study
pRG180	P_{N25}-His$_6$-LZ(0)-*virA*(*aa426-711*)(*G665D*) in pYW15b, Ap^r	This study
pTarA2	P_{N25}-*tar*(*aa1-214*)-*virA*(*aa281-829*) in pYW15b, Ap^r	This study
pTarA3	P_{N25}-*tar*(*aa1-214*)-*virA*(*aa282-829*) in pYW15b, Ap^r	This study
pTarA4	P_{N25}-*tar*(*aa1-214*)-*virA*(*aa283-829*) in pYW15b, Ap^r	This study
pTarA6	P_{N25}-*tar*(*aa1-214*)-*virA*(*aa285-829*) in pYW15b, Ap^r	This study
pTarA7	P_{N25}-*tar*(*aa1-214*)-*virA*(*aa286-829*) in pYW15b, Ap^r	This study
pTarA8	P_{N25}-*tar*(*aa1-214*)-*virA*(*aa287-829*) in pYW15b, Ap^r	This study
pTarIA3	P_{N25}-*tar*(*aa1-215*)-*virA*(*aa282-829*) in pYW15b, Ap^r	This study
pRG216	P_{N25}-*tar*(*aa1-214*)-*virA*(*aa283-829*)(*T154I*) in pYW15b, Ap^r	This study
pRG193	*virA*(*E295Q*) in pYW15b, Ap^r	This study
pRG194	*virA*(*E299Q*) in pYW15b, Ap^r	This study

these inputs have focused on several critical observations. First, the periplasmic domain of VirA was predicted to contain almost exclusively α-helices, much like the periplasmic domain of the methyl-accepting chemotaxis proteins (MCPs) Tar and Trg in *E. coli*. A 15-amino-acid segment in the VirA periplasmic domain is strongly homologous to a periplasmic domain of Trg believed to be the binding site of the ribose-binding protein (10). Second, mutations in this region of VirA abolish the interaction between VirA and the sugar-binding protein ChvE (38, 46). Finally, transmembrane signaling in *E. coli* chemotaxis has been tied to a sliding motion of one helix of a central four-helix bundle toward the cytoplasm (15). Taken together, these results suggest that VirA may share a signaling mechanism similar to that of the MCPs for pH/sugar perception.

Accordingly, VirA, with its well-defined signals, appeared to offer a unique opportunity where the mechanisms of periplasmic (pH/sugar) and cytoplasmic (phenol) perception converge to enable an integrated output response. Here we report construction of a series of VirA chimeras with the LZ of GCN4 or the periplasmic domain of Tar to specifically probe the input from each signaling domain. The results strongly suggest a signaling model built on a helix sliding/assisted rotation that allows the integrated transmission of information from the diverse input signals.

MATERIALS AND METHODS

Bacterial strains and plasmids. The bacterial strains and plasmids used in this study are listed in Table 1. *E. coli* strains XL1-Blue (Stratagene) and DH5α (Invitrogen) were used for routine cloning. *A. tumefaciens* strains were grown at 28°C in Luria-Bertani medium or induction medium (pH 5.5) (11) containing D-(−)-fructose as the carbon source. Additional supplements, such as antibiotics, AS, glucose, and isopropyl-β-D-thiogalactoside (IPTG), were added when appropriate as indicated below.

LZ(4/3/0)-*virA*(*aa426-829*)(*G665D*) chimeras were constructed using the PCR-ligation-PCR mutagenesis method (1). pYW59, pYW60, and pYW61b containing LZ(4/3/0)-*virA*(*aa294-829*)(*G665D*) (51) were used as templates for primary PCR. The PCR products amplified by using KA (5′-ATTCAGCTTCTTGAACTCGCC ACC-3′) and KB (5′-GCGGTACCCTACGTCTTGATTTTGGTTAG-3′) were treated with T4 DNA kinase to generate phosphates at the ends and were subsequently ligated with PCR fragments amplified by using LA (5′-GCGAATTCATT AAAGAGGAGAA-3′) and LB4 (5′-CTTCAGTGCGTCGACCAGCTTCTTC-3′), LB3 (5′-CAGTGCGTCGACCAGCTTCTTCAGT-3′), or LB0 (5′-GACCAG CTTCTTCAGTCTTGC-3′). Desired products containing LZ(4/3/0)-*virA*(*aa426-829*)(*G665D*) were amplified by using LA and KB with the ligation mixtures as templates, and then the 1.4-kb PCR fragments were digested with EcoRI/KpnI and cloned into pYW15b to obtain pRG95, pRG96, and pRG98. To construct LZ(4/3/0)-*virA*(*aa426-711*)(*G665D*) fusions, PCR were performed using LA and YL004 as the primers and pRG95, pRG96, and pRG98 as the templates. The PCR products were digested with EcoRI/Acc65I and cloned into pYW15b to obtain pRG178, pRG179, and pRG180. To create pRG150 containing P_{virB}-*lacZ* and *lacI*^{q}, pET24a (Novagen) was cut with DrdI and blunt ended by using the Klenow fragment and then digested with XbaI to release the *lacI*^{q} fragment. It was then ligated with EcoRI (blunt ended)/XbaI-digested pJZ4 to obtain pRG150.

Recombinant PCR were used to create the *tar-virA* fusions. Two primary PCR were performed separately. (i) TarN (5′-CACAGAATTCATTAAAGAGGAG AAATTAACTATGATTAACCGTATCCGC-3′) and TarI (5′-ACGGCGAAT GCCGTACCACGCCAC-3′) or TarAI (5′-CATACGGCGAATGCCGTACCA CGC-3′) were used to amplify *tar*(*aa1-214*) or *tar*(*aa1-215*) from the chromosomal DNA of *E. coli* strain DH5α, and (ii) pVRA8 containing wild-type *virA* was used as the template with VirAC (5′-GCAGGTACCGCAACTCTACGTC TTGAT-3′) and individual primers specific for *virA* fusions to create various *virA* fragments which had 16 bp complementary to the DNA sequence of the C

terminus of Tar(aa1-214) or Tar(aa1-215). The PCR products of these primary PCR were gel purified and mixed as templates for a secondary PCR with TarN and VirAC as the primers. The secondary PCR products were digested with EcoRI/KpnI and cloned into pYW15b after the P_{N25} promoter to obtain pTarA2, pTarA3, pTarA4, pTarA6, pTarA7, pTarA8, and pTarIA3. A T154I mutation was introduced into pTarA4 by site-specific mutagenesis using a similar recombinant PCR method with primers TarN, T154IS (5′-GCTTATTTCGCTC AGCCAATCCAGGGAATGCAAAAT-3′), T154AI (5′-ATTTTGCATTCCCT GGATTGGCTGAGCGAAATAAGC-3′), and VirAC.

Site-specific mutagenesis was also performed on pVRA8 using VirAC and VirAN (5′-GCAGAATTCAAGTCACCCGACGATTTGG-3′), which are specific sense and antisense primers containing the desired mutation, to generate *virA*(*E295Q*) and *virA*(*E299Q*). Subsequently, these PCR fragments were cloned into pYW15b as EcoRI/KpnI pieces to obtain pRG193 and pRG194.

β-Galactosidase assays for *vir* gene induction. To analyze *vir* expression in *A. tumefaciens*, induction assays were conducted as described previously (17). To determine the 50% effective doses of individual constructs, various AS concentrations were used to induce *vir* expression, and the induction curves were fitted to a modified Hill equation.

In vivo protein phosphorylation. In vivo ^{32}P labeling of VirA and VirG proteins was performed as described previously (34). *Agrobacterium* strains were cultured in phosphate-deficient induction medium for overnight phosphate starvation (12 h). Then $H_3{}^{32}PO_4$ (NEN Dupont) was added at a specific activity of 30 μCi/ml. After 3 h of labeling, the bacteria were harvested and lysed by brief sonication on ice. The six-His-tagged proteins were purified from the clarified lysates using Ni-nitrilotriacetic acid resins according to the QIAGEN protocol, using 500 mM imidazole for elution. The eluants were resolved by 10% Tris-glycine sodium dodecyl sulfate-polyacrylamide gel electrophoresis (Invitrogen) and electroblotted onto polyvinylidene difluoride (NEN Dupont) membranes for visualization by phosphorimaging (Amersham) and Western blot analysis using anti-penta-His monoclonal antibody (QIAGEN) (34).

RESULTS

Activation and coil orientation in the VirA linker. As shown in Fig. 1A, two helical coiled-coil-like regions, Helix-C and Helix-D, appear in secondary structure predictions in the VirA linker domain (50, 51). The amphipathic region Helix-C, located at the N terminus of the linker domain, is critical for signal transduction, and a ratchet model involving the rotation of the helices within the VirA dimer has been proposed (51). Helix-D is located at the C terminus of the linker, extending the helix directly into the conserved kinase helix of the HKs. The same pattern of coiled coils is common (40), as shown for Sln1 and ArcB in Fig. 1A, with a HAMP domain or P-type amphipathic helices preceding the kinase domain (5, 56). Helix rotation has also been suggested for osmosensor kinase Sln1 activation (44), and sequence alignment of Helix-D from VirA with Sln1 revealed a similar amphiphilic coiled-coil signature (Fig. 1B).

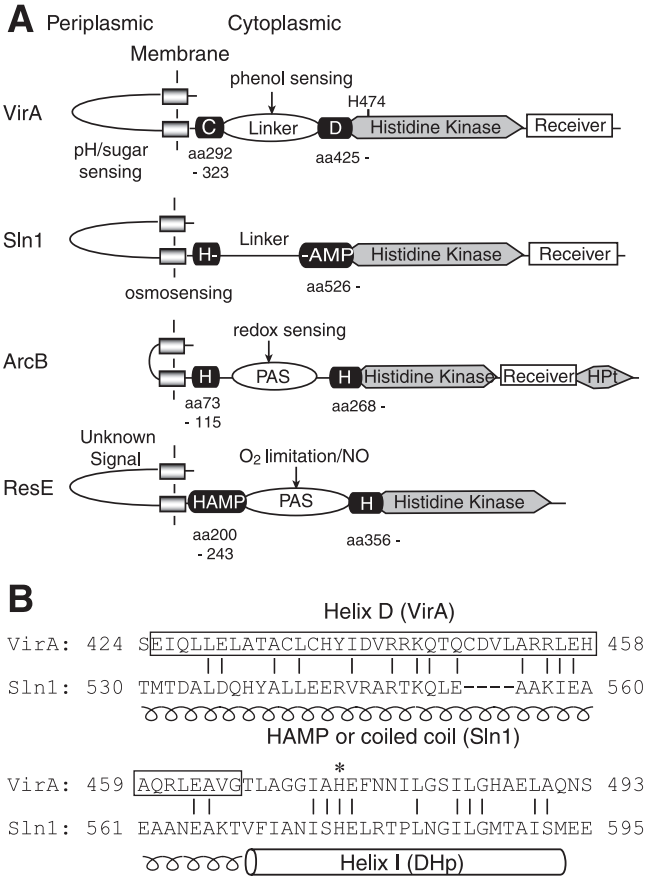

FIG. 1. Domain organization of long histidine kinases. (A) Two coiled-coil-like regions flanking the cytoplasmic linker domain are common in long histidine kinases. Helix-C (C) and Helix-D (D) were identified in VirA; HAMP domains or other predicted helical regions (H) were identified in Sln1, ArcB, and ResE. (B) Sequence comparison of VirA Helix-D with the coiled-coil in Sln1. Sequences were aligned with ClustalW. The cylinder indicates the conserved helix from the dimerization and DHp domain, and the conserved histidine residue is indicated by an asterisk; the box indicates the predicted Helix-D; and the spiral indicates the HAMP domain and coiled-coil regions in Sln1.

A similar LZ fusion strategy (14, 51) was developed to test the importance of rotational positioning in Helix-D (Fig. 2A). Any rotation within the coiled-coil dimer alters the helix interface, typically assigned to the hydrophobic residues located at the *a* and *d* positions of the heptad repeat sequences. The LZ domain of yeast transcription factor GCN4, a coiled coil with a large negative folding free energy, was fused at the N terminus of the flexible Helix-D to conformationally bias the interface in register with GCN4. Accordingly, insertion of three or four residues at the fusion point between GCN4 and Helix-D could force conrotatory repositioning of the Helix-D interface (Fig. 2A). The VirA allele encoding a G665D substitution (31), designated constitutively "on," was used to construct the chimeras because the wild-type VirA truncated at Helix-D (KR, *k*inase and *r*eceiver domains; amino acids 426 to 829) showed relatively low activity (data not shown). As observed with the Helix-C fusions reported previously (51), the expression of P_{virB}-*lacZ* mediated by these Helix-D fusions was indeed dependent on the putative Helix-D interface (Fig. 2B and C). LZ(4)-KR^{on} and LZ(0)-KR^{on} (KR^{on}, VirA aa426-829/G665D) were active in *vir* expression, while LZ(3)-KR^{on} was not (Fig. 2B). Removal of the receiver domain resulted in significantly higher activity for LZ(4)-K^{on} and LZ(0)-K^{on} (Fig. 2C), and the dependence on the number of inserted residues remained the same; LZ(3)-K^{on} again was inactive. Similar LZ(0/3/4) fusions at a different fusion point outside of Helix-D (amino acid 314) showed no difference in kinase activity (data not shown). Therefore, like Helix-C, the helical interface of Helix-D correlates with kinase activity, and the rotation of Helix-D may well directly regulate kinase output. Interestingly, the activity difference between the active alleles, LZ(4)-K^{on} and LZ(0)-K^{on}, is much greater than the difference between the corresponding fusions containing the receiver domain (Fig. 2B and

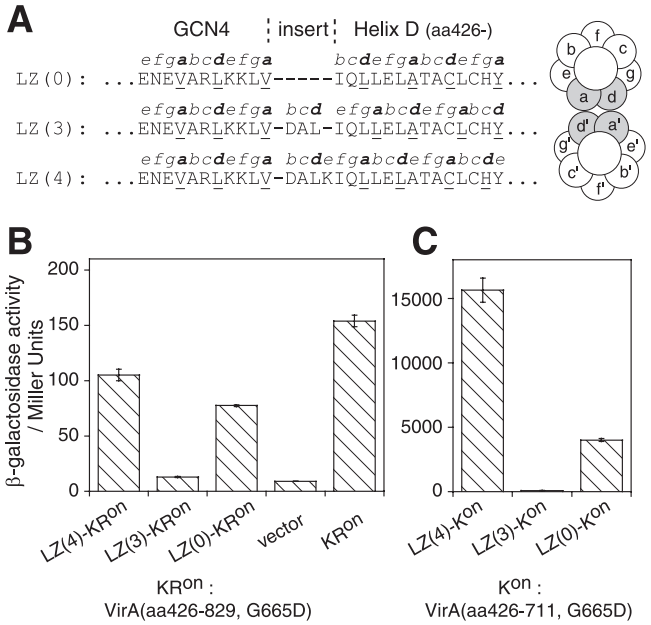

FIG. 2. Activity of LZ–Helix-D chimeras depends on the register of the LZ fusion. (A) Sequences of LZ–Helix-D chimeras and wheel representation of coiled-coil packing. The heptad repeating pattern of coiled coils is indicated by *a* through *g*. The hydrophobic core residues (*a* and *d*) enforced by LZ of GCN4 are highlighted to show different Helix-D interfaces due to the insertion sequence between LZ and Helix-D. (B) P_{virB}-*lacZ* expression of LZ-KR^{on}(aa426-829, G665D) fusions. A348-3(pSW209Ω) strains containing pRG95, pRG96, pRG98, pYW15b, and pRG100 (left to right) were assayed for β-galactosidase activity in the absence of AS. (C) P_{virB}-*lacZ* expression of LZ-K^{on}(aa426-711, G665D) fusions. These chimeras are highly active so *lacI*^{q} was introduced to induce chimera expression only during induction. A348-3(pRG150) strains containing pRG178, pRG179, and pRG180 were assayed in the presence of 200 μM IPTG.

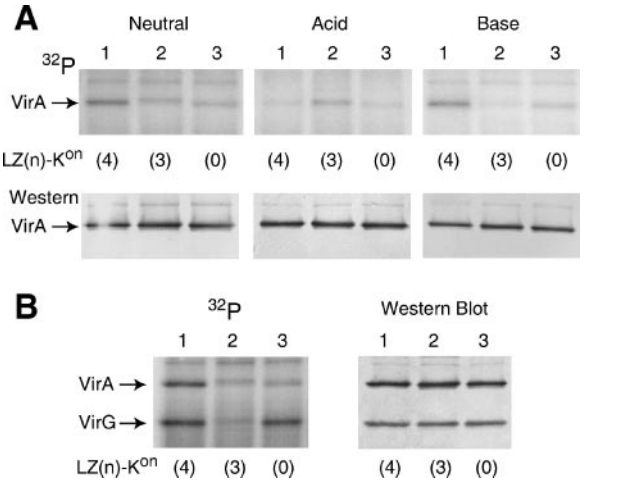

FIG. 3. In vivo phosphorylation of LZ–Helix-D chimeras. The phosphorylation patterns are shown in the ^{32}P panel, and the protein expression profiles detected by Western blotting using anti-His antibody are shown in the Western blot panel. (A) Chemical stability of phosphate on the chimeras. A348-3(pRG150) strains carrying the plasmids indicated were labeled with $H_3{}^{32}PO_4$ in the presence of 200 μM IPTG. Lane 1, pRG178; lane 2, pRG179; lane 3, pRG180. Three identical membranes were incubated with Tris-buffered saline (pH 7.0) (Neutral), 1 M HCl (Acid), and 3 N NaOH (Base) for 2 h at room temperature prior to phosphorimaging and Western blot analysis. (B) In vivo phosphorylation of both the LZ-VirA chimera and VirG. A136(pJM6) strains containing the plasmids mentioned above were analyzed.

2C), suggesting that the receiver domain may well play a role in regulating the rotational interface.

Is kinase phosphorylation correlated with LZ(0/3/4) fusions? As shown in Fig. 3A, in vivo phosphorylation of the LZ fusions described above resulted in greater phosphorylation for LZ(4)-K^{on} than for LZ(0)-K^{on}, consistent with the observed *vir* expression. Protein expression, as determined by Western blot analysis, did not correlate with the difference in autokinase activity. Interestingly, LZ(3)-K^{on} was phosphorylated, even though no *vir* expression was observed; however, the phosphorylated protein was stable to acid and labile to base, while the phosphates on LZ(4)-K^{on} and LZ(0)-K^{on} displayed an acid lability and base stability most characteristic of a histidyl phosphate. Hence, the phosphorylation observed for LZ(3)-K^{on} appears not to be on a histidine residue and to be physiologically less relevant to the kinase activity. Furthermore, the cognate response regulator VirG was phosphorylated only in the presence of the active VirA fusion proteins LZ(4)-K^{on} and LZ(0)-K^{on}, while LZ(3)-K^{on} did not induce significant VirG phosphorylation (Fig. 3B). Taken together, the results show that the phosphorylation status of the VirA kinase correlates with switching Helix-D interfaces.

Can Tar-VirA hybrids respond to AS? Given the similarity between the periplasmic domains of VirA and MCPs, Tar-VirA hybrids were constructed to explore the potential for conserved transmembrane signaling mechanisms. Multiple fusion points following the second transmembrane region (TM2) were chosen. As shown in Fig. 4, all of the Tar-VirA hybrids were inactive in the absence of AS but retained inducible activity (Fig. 4B). The striking observation was that TarA2, TarA3, and TarA4 showed a position-dependent increase in kinase activity. Each consecutive deletion of one residue along the TM2 helix is consistent with rotation of the helix by ~100°. Apparently, the difference is not caused by different truncation points as TarIA3, carrying the same truncation as TarA3 but with an additional residue from Tar to keep the helical register the same as TarA2, had a *vir* expression level similar to that of TarA2. Moreover, TarA6, TarA7, and TarA8, with four residues (approximately one turn of a helix) less than the corresponding TarA2, TarA3, and TarA4, displayed a similar pattern of increasing activity (Fig. 4B). The AS sensitivity also changed with these fusions; the concentration required to reach half-maximal activity (50% effective dose) for TarA4 was ~40 μM and thus TarA4 was more sensitive than the wild type, the concentration required to reach half-maximal activity for TarA3 was ~120 μM, and TarA2 required significantly higher AS concentrations (Fig. 4C and Table 2).

Can Tar-VirA hybrids respond to aspartate? Without the periplasmic domain, the Tar-VirA hybrids did not respond to glucose or aspartate alone (data not shown). However, in the presence of AS, the activities of TarA2, TarA3, and TarA4 were all suppressed by aspartate relative to the VirA activity with or without sugar (Fig. 5A). Moreover, this suppression was dose dependent, and the aspartate concentration required for half-maximal repression was similar (Fig. 5B), 0.5 to ~1

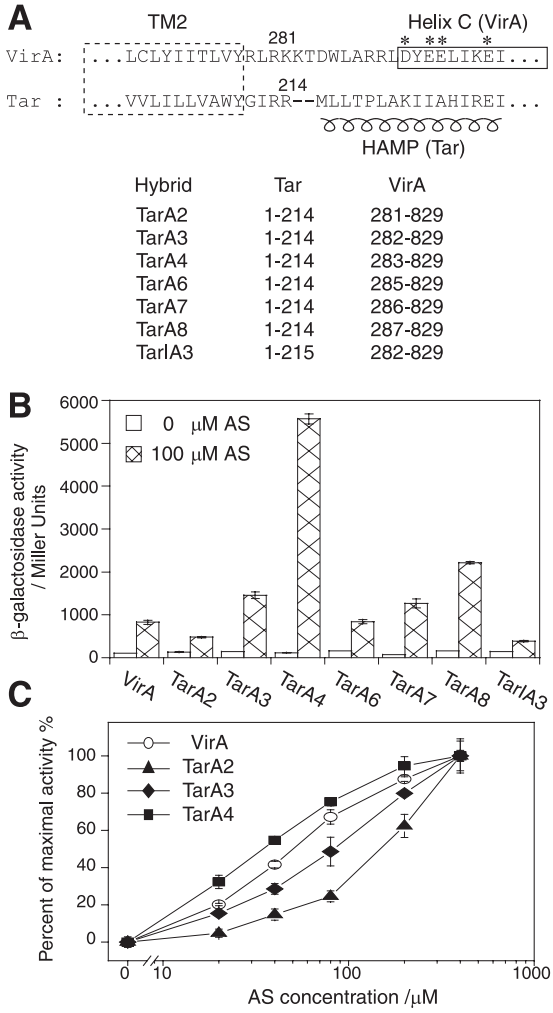

FIG. 4. P_{virB}-*lacZ* expression by Tar-VirA chimeras. (A) Sequence of Tar-VirA fusions. The HAMP domain from Tar is indicated by the spiral, while Helix-C from VirA is indicated by the box. Negatively charged residues (indicated by asterisks) are clustered at the start of Helix-C. (B and C) P_{virB}-*lacZ* expression (B) and AS dose response (C) by Tar-VirA chimeras. A136(pRG109) strains carrying pVRA8(VirA) or corresponding TarA plasmids were assayed in induction medium containing the noninducing sugar fructose (4) as the carbon source. All the Tar-VirA fusions were placed behind the P_{N25} promoter, while *virA* was expressed under control of its own promoter.

mM, and comparable to that for the Tar-EnvZ fusion Taz1 (49). The T154I allele of Tar has been shown to mimic the aspartate occupancy and give a basal activity that still responds to aspartate (25). Reduction of activity was apparent for TarA4(T154I) at high and low AS concentrations (Fig. 5C). As observed for the sugar response of wild-type VirA, aspartate also altered the AS sensitivity of TarA fusions (Fig. 5D and Table 2). Therefore, the Tar-VirA hybrids respond specifically to the natural ligand of Tar, but they do so via suppression rather than induction.

A high density of negatively charged acidic residues appears to be important for the dynamics of the helices in the adaptation domain of Tar (42). Similar clusters of glutamate and aspartate residues are present in the Helix-C/D domains, especially at the beginning of Helix-C (Fig. 4A). The dynamics of Helix-C/D could contribute to the rotation/sliding motions involved in signal transmission. To test for the importance of these residues, two negatively charged residues were neutralized by E-to-Q substitutions at position 295 (E295Q) and at a position four residues further along the putative helix (E299Q). Both substitutions enhanced phenol induction in the absence of glucose (Fig. 6), consistent with a model indicating that the electrostatic interactions within these helices restrict the phenol-induced signaling motions. Apparently, monosaccharide perception can override the effects of these mutations since the mutants were as active as the wild type in the presence of glucose (Fig. 6).

DISCUSSION

In our attempts to identify common mechanistic controls within the complex regulatory architecture of the HK sensors, the mediator of pathogenic commitment in *A. tumefaciens*, VirA, is distinctive for many reasons. Most notably, multiple molecular signals are perceived and processed by this membrane protein. While this signal multiplicity adds complexity, two separate signal input domains have been described. The periplasmic domain resembles the proposed piston-like "sliding" chemoreceptors, and the cytoplasmic domain has been implicated in "rotational" motions (51). Therefore, VirA offers the unique opportunity to evaluate how these motional dynamics might function cooperatively in signal integration and transmission.

For 189 class I HKs studied by Singh et al. (40), coiled coils immediately preceding the histidine-containing H-box were predicted in 76% of the sequences. The coiled-coil region, usually corresponding to the HAMP motif and known as the P-type linker, is proposed to play a critical role in HK signal transduction (5, 56). Although the P-type linker was not identified in VirA (56), the coiled-coil-like Helix-D occurs in a similar region just before the H-box. We have now shown that fusion of an LZ domain in register with Helix-D gives VirA chimeras whose activity is dependent on the rotational interface. Similar results were obtained for the coiled coil in the yeast osmosensor Sln1, implying that there is a common rotation mechanism (44). Recent nuclear magnetic resonance analyses of a HAMP domain revealed the structural basis of the rotation mechanism in which the interhelical packing within a homodimeric four-helix bundle is altered by helix rotational motions (20).

TABLE 2. Fifty percent effective doses of Tar-VirA chimeras in response to AS

Strain[a]	50% Effective dose (μM) with[b]:	
	0 mM Asp	2.5 mM Asp
VirA	51 ± 8	48 ± 6
TarA2	—[c]	—[c]
TarA3	128 ± 20	155 ± 27
TarA4	38 ± 1	63 ± 3

[a] Strain A136(pRG109) constructs containing pVRA8, pTarA2, pTarA3, and pTarA4 were assayed.
[b] The 50% effective dose was determined by fitting the AS induction curve to a modified Hill equation.
[c] At the highest AS concentration tested, TarA2 did not reach the maximal plateau activity. Thus, a good fit was not available.

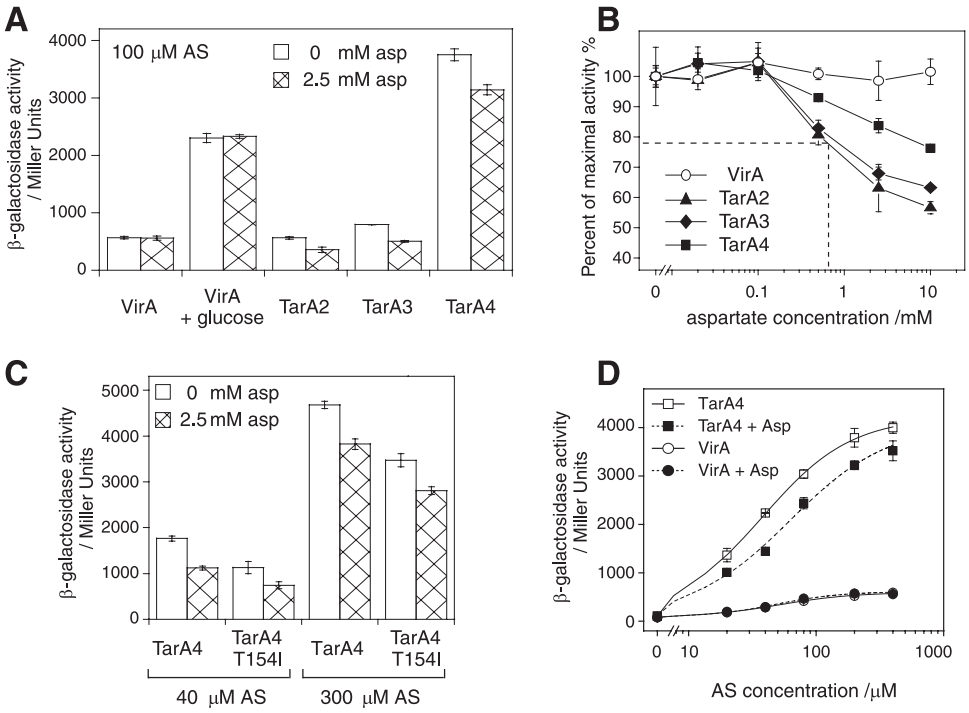

FIG. 5. P_{virB}-*lacZ* expression of Tar-VirA chimeras in response to aspartate. A136(pRG109) strains carrying pVRA8(VirA) or pRG216(TarA4, T154I) or corresponding TarA plasmids were assayed. (A and C) Comparison of activity in the absence or presence of 2.5 mM aspartate. (B) Aspartate dose response expressed as a percentage of the maximal activity. (D) AS dose response affected by the presence of 2.5 mM aspartate. Curve fitting was done as described in Materials and Methods.

In our studies, in vivo phosphorylation of LZ–Helix-D chimeras argued for the dependence of histidine phosphorylation on the rotational interface. Hence, the postulated rotation of the coiled-coil-like Helix-D may regulate kinase phosphorylation directly, possibly via optimal positioning of the histidine residue in the catalytic ATP-binding (CA) subdomain of the kinase. In this context, the structure of the cytoplasmic portion of another histidine kinase implies that the coiled-coil region extends into the conserved histidine-containing helix of the dimerization and histidine phosphotransfer (DHp) subdomains (28). Even though ATP readily binds to the CA domain, a rotation of the coiled-coil region could allow access of the bound ATP to the histidine.

HAMP domains in typical HKs, however, consist of two helical regions, one extending to the kinase domain, as in Helix-D, and the other connecting to the transmembrane region, as in Helix-C of VirA. LZ–Helix-C fusions further supported rotational positioning as necessary for activation (51). Since the LZ–Helix-C fusions lost the ability to respond to AS, even with an intact AS-sensing linker domain, it was hypothesized that helix rotation was dependent on phenol activation and that LZ fusions restricted this movement (51). An alternative interpretation is that the LZ fusions generate periodic perturbations of the dimer interface different from the proposed rotational interfaces, resulting in oscillating activities. However, our studies of the Tar-VirA chimeras, with fusion points just behind TM2, can also be rationalized by a rotation mechanism of Helix-C. Consecutive deletions of residues at the fusion points increased activity (TarA2, TarA3, and TarA4), and the same pattern was repeated with further deletions across a second helical turn (residues in TarA6, TarA7, and TarA8). However, unlike the LZ fusions which were independent of AS, all the Tar-VirA fusions remained dependent on AS induction, consistent with previous reports of active Tar-VirA hybrids (32, 47). Since the four-helix bundle structure of Tar was suggested to be rather flexible and dynamic, allowing piston-like sliding and/or rotation (36, 58), the Tar fusions should not have a folding energy as strong as that of GCN4 and therefore are not sufficient to lock Helix-C into a constitutive active/inactive interface. However, the Tar fusion could alter the phenol-induced rotation by incrementally changing the energy barrier for each helix position.

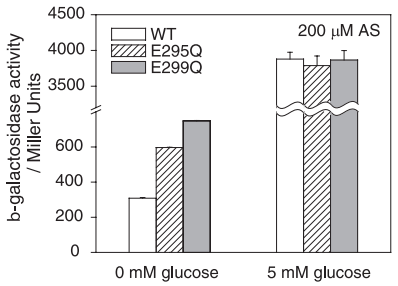

FIG. 6. Activity of VirA mutants with E residues in Helix-C replaced by Q. A136(pRG109) strains carrying pVRA8 (VirA wild type) (WT), pRG193 (E295Q), and pRG194 (E299Q) were assayed.

The rotational movements implied for both Helix-C and Helix-D suggested that signal-induced conformational changes

FIG. 7. Alignment of VirA linker with known GAF structures. The sequence alignment is from the Pfam database and was refined based on structures (protein data bank ID 1MC0, 1YKD, 1VHM, and 1F5M). H and E represent α-helices and β-strands observed in the structure, respectively. The secondary structure of the VirA linker was predicted by the SAM-T02 method. Predicted α-helices and β-strands are indicated by cylinders and arrows. The dotted arrow indicates a β-strand that is not conserved among GAF structures. Residues with remote homology are the following colors: blue, hydrophobic and aromatic residues (L, I, V, M, C, A, F, and W); red, charged residues (D, E, K, and R); orange, G; yellow, P; green, S, T, N, and Q.

might propagate from Helix-C to Helix-D within a higher-order structure. Indeed, central four-helix bundle structures are present in the signaling and adaptation subdomains of the chemoreceptor Tar/Tsr (15, 58), the HAMP domain (20), the phototaxis receptor sensory rhodopsin II (NpSRII) from *Haloarchaea* (33), and the homodimer of DHp domains (28, 43). Therefore, Helix-C and Helix-D within a VirA homodimer might be arranged as a four-helix bundle, and this more complex arrangement opens additional modes of signal transmission. Indeed, clockwise rotation together with a tilt of the signaling helix has been suggested for the transmembrane signaling in the phototaxis receptor rhodopsin NpSRII (33).

Even though the VirA linker domain exhibits low sequence homology to known structures, recent advances in bioinformatics have improved the detection of remotely homologous sequences significantly. Searching the VirA linker sequence against the SUPERFAMILY library (www.superfam.org) (18) and the Pfam database (7) resulted in identification of the linker as a GAF-like domain. The GAF domains, distantly related to the PAS domains (3, 45), appear to be a large family of small-molecule-binding domains that generally do not display strong sequence conservation but are widely distributed in signaling proteins, including the HKs (3, 6). The predicted secondary structure elements of the VirA linker aligned very well with known GAF structures (Fig. 7), which contain a central antiparallel β-sheet flanked by α-helices at both faces (19, 26, 29). Helix-C and Helix-D, corresponding to the α1- and α4-helices (Fig. 7), are packed against each other in the GAF structure. In the GAF structure CodY, these two helices were found to form a four-helix bundle within the homodimer (26). This homology comparison leads to a model where phenols, or other regulatory elements including the receiver domain of VirA, could associate with the putative GAF fold of the linker to regulate the rotational interface for signaling.

Since Helix-C connects directly to TM2, transmembrane signaling from periplasmic pH/sugar perception would exert its conformation change on Helix-C. Indeed, all the Tar-VirA chimeras responded to aspartate like wild-type VirA responded to glucose. For example, aspartate did not activate the chimera in the absence of phenols but rather altered the maximal level and sensitivity of phenol induction. Therefore, these chimeras are able to successfully integrate aspartate sensing by the Tar receptor domain within cytoplasmic phenol sensing. Curiously, and in contrast to the enhanced phenol response mediated by glucose, aspartate lowered the maximal activity and reduced phenol sensitivity. As the piston-like movement in transmembrane signaling of Tar/Tsr is most consistent with sliding along the TM2 helix toward the cytoplasm (15), the result suggests that oppositely directed piston-like sliding toward the periplasmic space might operate in wild-type VirA for pH/sugar signaling. Maltose also activates Tar through maltose-binding protein, but while maltose had no effect on the AS response of Tar-VirA chimeras (data not shown), this response may well require the maltose-binding protein from *E. coli*.

Two limiting models emerge from the observation that both VirA and the Tar-VirA chimeras are capable of integrating the signals from both input domains. First, it is possible that piston-like sliding of Helix-C could change the conformation within the phenol-binding site to increase the binding affinity and enhance the phenol sensitivity. Alternatively, the piston motion could modulate transduction rather than perception, altering helical rotation within the putative four-helix bundle formed by the Helix-C/D homodimer. A change in signal sensitivity is certainly not always associated with a change in the

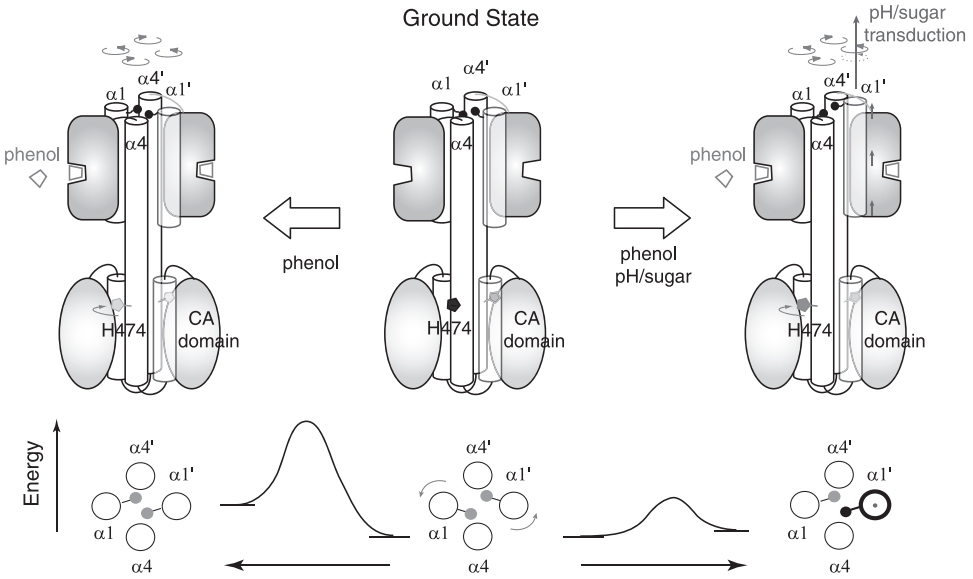

FIG. 8. Signal integration model for VirA signaling. A central four-helix bundle formed by Helix-C and Helix-D (α1 and α4 in the predicted GAF structure) is critical for both periplasmic and cytoplasmic signaling. Helix-D is directly connected to the histidine-containing helix of the DHp domain, and the rotational motion modulates the phosphorylation of the histidine residue (pentagon). Phenol perception by the small-molecule-binding GAF structure of the linker domain is postulated to initiate the rotation within the four-helix bundle, but the rotation energy barrier is high due to the restriction by the periplasmic domain, possibly via the positioning of clustered charged residues. The periplasmic sensing of pH or sugar induces sliding of signaling helices to lower the energy barrier for rotation to enhance the phenol response.

signal molecule-binding site. For instance, methylation of adaptation sites in the cytoplasmic domain of Tar alters the receptor sensitivity to aspartate, while the periplasmic aspartate-binding sites remain the same (41). Rather, the transduction is believed to be altered by methylation of certain glutamate residues. Electrostatic interactions within the adaptation domain have been suggested to modulate the stabilities and packing interactions of adjacent helices within the four-helix bundle (42). Helical sliding could change interhelical packing or the interactions of the helices with other VirA regions to facilitate or restrict the helical rotation and enhance the response to glucose for VirA or reduce the response to aspartate for the Tar-VirA chimeras. As seen in the different AS responses of TarA2, TarA3, and TarA4, perturbing the energy barrier for helix rotation by modifying fusion points could certainly alter both maximal induction and phenol sensitivity.

With this perspective, we tested the electrostatic interactions within the highly charged region at the start of Helix-C. E-to-Q substitutions at residues i and $i + 4$ along the predicted helix significantly increased AS induction in the absence of glucose. If these residues contribute to the rotation-restricting electrostatic interactions, E-to-Q mutations at key residues would reduce the barrier. Piston-like helical sliding induced by sugar sensing could reposition these residues by helix sliding and also reduce the electrostatic barrier to enable helical rotation.

Taken together, these results suggest that VirA might accommodate separate inputs by integrating rotation and piston mechanisms within its linker domain. We propose that helical rotation within the central four-helix bundle formed by Helix-C and Helix-D is induced by phenol sensing and that piston-like sliding of Helix-C is initiated by the periplasmic sensing of sugar and low pH. These combined inputs are summarized in Fig. 8, where a sliding-modulated helical rotation model is proposed for signal integration. In the absence of periplasmic signals, the cumulative effect of electrostatic interactions and helix packing in wild-type VirA restricts central helical rotation, but high phenol concentrations are able to overcome the activation barrier required for helical rotation and histidine reorientation for phosphorylation (Fig. 8, left diagram). In the presence of periplasmic pH and sugar signals, helical sliding changes the helical packing and relieves the rotation-restricting interactions to both enhance the phenol response and lower the required phenol concentration (Fig. 8, right diagram). This elegantly simple model for signal output can now be used to design physical tests for the proposed motions and even to engineer new chimeras for alternate signaling strategies.

ACKNOWLEDGMENTS

We are indebted to Andrew Binns and his laboratory at the University of Pennsylvania for resources, insight, and advice.

We acknowledge the valuable support of NIH grant GM47369.

REFERENCES

1. **Ali, S. A., and A. Steinkasserer.** 1995. PCR-ligation-PCR mutagenesis: a protocol for creating gene fusions and mutations. BioTechniques **18:**746–750.
2. **Amemura, M., K. Makino, H. Shinagawa, and A. Nakata.** 1990. Cross talk to the phosphate regulon of *Escherichia coli* by PhoM protein: PhoM is a histidine protein kinase and catalyzes phosphorylation of PhoB and PhoM-open reading frame 2. J. Bacteriol. **172:**6300–6307.
3. **Anantharaman, V., E. V. Koonin, and L. Aravind.** 2001. Regulatory potential, phyletic distribution and evolution of ancient, intracellular small-molecule-binding domains. J. Mol. Biol. **307:**1271–1292.
4. **Ankenbauer, R. G., and E. W. Nester.** 1990. Sugar-mediated induction of *Agrobacterium tumefaciens* virulence genes: structural specificity and activities of monosaccharides. J. Bacteriol. **172:**6442–6446.
5. **Aravind, L., and C. P. Ponting.** 1999. The cytoplasmic helical linker domain of receptor histidine kinase and methyl-accepting proteins is common to many prokaryotic signalling proteins. FEMS Microbiol. Lett. **176:**111–116.

6. **Aravind, L., and C. P. Ponting.** 1997. The GAF domain: an evolutionary link between diverse phototransducing proteins. Trends Biochem. Sci. **22:**458.
7. **Bateman, A., L. Coin, R. Durbin, R. D. Finn, V. Hollich, S. Griffiths-Jones, A. Khanna, M. Marshall, S. Moxon, E. L. L. Sonnhammer, D. J. Studholme, C. Yeats, and S. R. Eddy.** 2004. The Pfam protein families database. Nucleic Acids Res. **32:**D138–D141.
8. **Baumgartner, J. W., C. Kim, R. E. Brissette, M. Inouye, C. Park, and G. L. Hazelbauer.** 1994. Transmembrane signalling by a hybrid protein: communication from the domain of chemoreceptor Trg that recognizes sugar-binding proteins to the kinase/phosphatase domain of osmosensor EnvZ. J. Bacteriol. **176:**1157–1163.
9. **Bijlsma, J. J., and E. A. Groisman.** 2003. Making informed decisions: regulatory interactions between two-component systems. Trends Microbiol. **11:**359–366.
10. **Cangelosi, G. A., R. G. Ankenbauer, and E. W. Nester.** 1990. Sugars induce the Agrobacterium virulence genes through a periplasmic binding protein and a transmembrane signal protein. Proc. Natl. Acad. Sci. USA **87:**6708–6712.
11. **Cangelosi, G. A., E. A. Best, G. Martinetti, and E. W. Nester.** 1991. Genetic analysis of Agrobacterium. Methods Enzymol. **204:**384–397.
12. **Chang, C. H., and S. C. Winans.** 1992. Functional roles assigned to the periplasmic, linker, and receiver domains of the *Agrobacterium tumefaciens* VirA protein. J. Bacteriol. **174:**7033–7039.
13. **Chang, C. H., J. Zhu, and S. C. Winans.** 1996. Pleiotropic phenotypes caused by genetic ablation of the receiver module of the *Agrobacterium tumefaciens* VirA protein. J. Bacteriol. **178:**4710–4716.
14. **Cochran, A. G., and P. S. Kim.** 1996. Imitation of *Escherichia coli* aspartate receptor signaling in engineered dimers of the cytoplasmic domain. Science **271:**1113–1116.
15. **Falke, J. J., and G. L. Hazelbauer.** 2001. Transmembrane signaling in bacterial chemoreceptors. Trends Biochem. Sci. **26:**257–265.
16. **Fisher, S. L., W. H. Jiang, B. L. Wanner, and C. T. Walsh.** 1995. Cross-talk between the histidine protein-kinase Vans and the response regulator PhoB—characterization and identification of a Vans domain that inhibits activation of PhoB. J. Biol. Chem. **270:**23143–23149.
17. **Gao, R., and D. G. Lynn.** 2005. Environmental pH sensing: resolving the VirA/VirG two-component system inputs for *Agrobacterium* pathogenesis. J. Bacteriol. **187:**2182–2189.
18. **Gough, J., K. Karplus, R. Hughey, and C. Chothia.** 2001. Assignment of homology to genome sequences using a library of hidden Markov models that represent all proteins of known structure. J. Mol. Biol. **313:**903–919.
19. **Ho, Y.-S. J., L. M. Burden, and J. H. Hurley.** 2000. Structure of the GAF domain, a ubiquitous signaling motif and a new class of cyclic GMP receptor. EMBO J. **19:**5288–5299.
20. **Hulko, M., F. Berndt, M. Gruber, J. U. Linder, V. Truffault, A. Schultz, J. Martin, J. E. Schultz, A. N. Lupas, and M. Coles.** 2006. The HAMP domain structure implies helix rotation in transmembrane signaling. Cell **126:**929–940.
21. **Kox, L. F. F., M. M. S. M. Wosten, and E. A. Groisman.** 2000. A small protein that mediates the activation of a two-component system by another two-component system. EMBO J. **19:**1861–1872.
22. **Kwon, O., D. Georgellis, and E. C. Lin.** 2003. Rotational on-off switching of a hybrid membrane sensor kinase Tar-ArcB in *Escherichia coli*. J. Biol. Chem. **278:**13192–13195.
23. **Lee, K., M. W. Dudley, K. M. Hess, D. G. Lynn, R. D. Joerger, and A. N. Binns.** 1992. Mechanism of activation of Agrobacterium virulence genes: identification of phenol-binding proteins. Proc. Natl. Acad. Sci. USA **89:**8666–8670.
24. **Lee, K., Y. L. Tzeng, N. Liu, M. W. Dudley, and D. G. Lynn.** 1993. Possible evolutionary relationships in a signal transduction system. Pure Appl. Chem. **65:**1241–1248.
25. **Lee, L., and Y. Imae.** 1990. Role of threonine residue 154 in ligand recognition of the tar chemoreceptor in *Escherichia coli*. J. Bacteriol. **172:**377–382.
26. **Levdikov, V. M., E. Blagova, P. Joseph, A. L. Sonenshein, and A. J. Wilkinson.** 2006. The structure of CodY, a GTP- and isoleucine-responsive regulator of stationary phase and virulence in gram-positive bacteria. J. Biol. Chem. **281:**11366–11373.
27. **Maresh, J. M.** 2004. Ph.D. thesis. The University of Chicago, Chicago, IL.
28. **Marina, A., C. D. Waldburger, and W. A. Hendrickson.** 2005. Structure of the entire cytoplasmic portion of a sensor histidine-kinase protein. EMBO J. **24:**4247–4259.
29. **Martinez, S. E., S. Bruder, A. Schultz, N. Zheng, J. E. Schultz, J. A. Beavo, and J. U. Linder.** 2005. Crystal structure of the tandem GAF domains from a cyanobacterial adenylyl cyclase: modes of ligand binding and dimerization. Proc. Natl. Acad. Sci. USA **102:**3082–3087.
30. **McCullen, C. A., and A. N. Binns.** 2006. Agrobacterium tumefaciens and plant cell interactions and activities required for interkingdom macromolecular transfer. Annu. Rev. Cell Dev. Biol. **22:**101–127.
31. **McLean, B. G., E. A. Greene, and P. C. Zambryski.** 1994. Mutants of Agrobacterium VirA that activate *vir* gene expression in the absence of the inducer acetosyringone. J. Biol. Chem. **269:**2645–2651.
32. **Melchers, L. S., T. J. Regensburg-Tuink, R. B. Bourret, N. J. Sedee, R. A. Schilperoort, and P. J. Hooykaas.** 1989. Membrane topology and functional analysis of the sensory protein VirA of *Agrobacterium tumefaciens*. EMBO J. **8:**1919–1925.
33. **Moukhametzianov, R., J. P. Klare, R. Efremov, C. Baeken, A. Göppner, J. Labahn, M. Engelhard, G. Büldt, and V. I. Gordeliy.** 2006. Development of the signal in sensory rhodopsin and its transfer to the cognate transducer. Nature **440:**115.
34. **Mukhopadhyay, A., R. Gao, and D. G. Lynn.** 2004. Integrating input from multiple signals: the VirA/VirG two component system of *Agrobacterium tumefaciens*. ChemBioChem **5:**1535–1542.
35. **Palmer, A. G., R. Gao, J. Maresh, W. K. Erbil, and D. G. Lynn.** 2004. Chemical biology of multi-host/pathogen interactions: chemical perception and metabolic complementation. Annu. Rev. Phytopathol. **42:**439–464.
36. **Peach, M. L., G. L. Hazelbauer, and T. P. Lybrand.** 2002. Modeling the transmembrane domain of bacterial chemoreceptors. Protein Sci. **11:**912–923.
37. **Perego, M.** 1998. Kinase-phosphatase competition regulates Bacillus subtilis development. Trends Microbiol. **6:**366.
38. **Shimoda, N., A. Toyoda-Yamamoto, S. Aoki, and Y. Machida.** 1993. Genetic evidence for an interaction between the VirA sensor protein and the ChvE sugar-binding protein of Agrobacterium. J. Biol. Chem. **268:**26552–26558.
39. **Shimoda, N., A. Toyoda-Yamamoto, J. Nagamine, S. Usami, M. Katayama, Y. Sakagami, and Y. Machida.** 1990. Control of expression of Agrobacterium *vir* genes by synergistic actions of phenolic signal molecules and monosaccharides. Proc. Natl. Acad. Sci. USA **87:**6684–6688.
40. **Singh, M., B. Berger, P. S. Kim, J. M. Berger, and A. G. Cochran.** 1998. Computational learning reveals coiled coil-like motifs in histidine kinase linker domains. Proc. Natl. Acad. Sci. USA **95:**2738–2743.
41. **Sourjik, V., and H. C. Berg.** 2002. Receptor sensitivity in bacterial chemotaxis. Proc. Natl. Acad. Sci. USA **99:**123–127.
42. **Starrett, D. J., and J. J. Falke.** 2005. Adaptation mechanism of the aspartate receptor: electrostatics of the adaptation subdomain play a key role in modulating kinase activity. Biochemistry **44:**1550–1560.
43. **Stock, A. M., V. L. Robinson, and P. N. Goudreau.** 2000. Two-component signal transduction. Annu. Rev. Biochem. **69:**183–215.
44. **Tao, W., C. L. Malone, A. D. Ault, R. J. Deschenes, and J. S. Fassler.** 2002. A cytoplasmic coiled-coil domain is required for histidine kinase activity of the yeast osmosensor, SLN1. Mol. Microbiol. **43:**459–473.
45. **Taylor, B. L., and I. B. Zhulin.** 1999. PAS domains: internal sensors of oxygen, redox potential, and light. Microbiol. Mol. Biol. Rev. **63:**479–506.
46. **Toyoda-Yamamoto, A., N. Shimoda, and Y. Machida.** 2000. Genetic analysis of the signal-sensing region of the histidine protein kinase VirA of *Agrobacterium tumefaciens*. Mol. Gen. Genet. **263:**939–947.
47. **Turk, S. C., R. P. van Lange, E. Sonneveld, and P. J. Hooykaas.** 1993. The chimeric VirA-Tar receptor protein is locked into a highly responsive state. J. Bacteriol. **175:**5706–5709.
48. **Tzfira, T., and V. Citovsky.** 2002. Partners-in-infection: host proteins involved in the transformation of plant cells by Agrobacterium. Trends Cell Biol. **12:**121–129.
49. **Utsumi, R., R. E. Brissette, A. Rampersaud, S. A. Forst, K. Oosawa, and M. Inouye.** 1989. Activation of bacterial porin gene-expression by a chimeric signal transducer in response to aspartate. Science **245:**1246–1249.
50. **Wang, Y.** 1999. Ph.D. thesis. The University of Chicago, Chicago, IL.
51. **Wang, Y., R. Gao, and D. G. Lynn.** 2002. Ratcheting up *vir* gene expression in *Agrobacterium tumefaciens*: coiled coils in histidine kinase signal transduction. ChemBioChem **3:**311–317.
52. **Wang, Y., A. Mukhopadhyay, V. R. Howitz, A. N. Binns, and D. G. Lynn.** 2000. Construction of an efficient expression system for *Agrobacterium tumefaciens* based on the coliphage T5 promoter. Gene **242:**105–114.
53. **Ward, S. M., A. Delgado, R. P. Gunsalus, and M. D. Manson.** 2002. A NarX-Tar chimera mediates repellent chemotaxis to nitrate and nitrite. Mol. Microbiol. **44:**709–719.
54. **Watson, B., T. C. Currier, M. P. Gordon, M. D. Chilton, and E. W. Nester.** 1975. Plasmid required for virulence of *Agrobacterium tumefaciens*. J. Bacteriol. **123:**255–264.
55. **West, A. H., and A. M. Stock.** 2001. Histidine kinases and response regulator proteins in two-component signaling systems. Trends Biochem. Sci. **26:**369–376.
56. **Williams, S. B., and V. Stewart.** 1999. Functional similarities among two-component sensors and methyl-accepting chemotaxis proteins suggest a role for linker region amphipathic helices in transmembrane signal transduction. Mol. Microbiol. **33:**1093–1102.
57. **Winans, S. C., N. J. Mantis, C. Y. Chen, C. H. Chang, and D. C. Han.** 1994. Host recognition by the VirA, VirG two-component regulatory proteins of *Agrobacterium tumefaciens*. Res. Microbiol. **145:**461–473.
58. **Winston, S. E., R. Mehan, and J. J. Falke.** 2005. Evidence that the adaptation region of the aspartate receptor is a dynamic four-helix bundle: cysteine and disulfide scanning studies. Biochemistry **44:**12655–12666.
59. **Zhu, J., P. M. Oger, B. Schrammeijer, P. J. Hooykaas, S. K. Farrand, and S. C. Winans.** 2000. The bases of crown gall tumorigenesis. J. Bacteriol. **182:**3885–3895.